Clinical Cancer Research

A Phase I/II Study for Analytic Validation of ^{89}Zr-J591 ImmunoPET as a Molecular Imaging Agent for Metastatic Prostate Cancer

Neeta Pandit-Taskar[1,2], Joseph A. O'Donoghue[3], Jeremy C. Durack[1], Serge K. Lyashchenko[4,5], Sarah M. Cheal[1,4], Volkan Beylergil[1], Robert A. Lefkowitz[1,2], Jorge A. Carrasquillo[1,2], Danny F. Martinez[6], Alex Mak Fung[1], Stephen B. Solomon[1,2], Mithat Gönen[7], Glenn Heller[7], Massimo Loda[8], David M. Nanus[9], Scott T. Tagawa[9], Jarett L. Feldman[6], Joseph R. Osborne[1,2], Jason S. Lewis[2,4,5], Victor E. Reuter[10], Wolfgang A. Weber[1,2], Neil H. Bander[9,11], Howard I. Scher[6,9], Steven M. Larson[1,2,4], and Michael J. Morris[6,9]

Abstract

Purpose: Standard imaging for assessing osseous metastases in advanced prostate cancer remains focused on altered bone metabolism and is inadequate for diagnostic, prognostic, or predictive purposes. We performed a first-in-human phase I/II study of ^{89}Zr-DFO-huJ591 (^{89}Zr-J591) PET/CT immunoscintigraphy to assess performance characteristics for detecting metastases compared with conventional imaging modalities (CIM) and pathology.

Experimental Design: Fifty patients with progressive metastatic castration-resistant prostate cancers were injected with 5 mCi of ^{89}Zr-J591. Whole-body PET/CT scans were obtained, and images were analyzed for tumor visualization. Comparison was made to contemporaneously obtained bone scintigraphy and cross-sectional imaging on a lesion-by-lesion basis and with biopsies of metastatic sites.

Results: Median standardized uptake value for ^{89}Zr-J591–positive bone lesions ($n = 491$) was 8.9 and for soft-tissue lesions ($n = 90$), it was 4.8 ($P < 0.00003$). ^{89}Zr-J591 detected 491 osseous sites compared with 339 by MDP and 90 soft-tissue lesions compared with 124 by computed tomography (CT). Compared with all CIMs combined, ^{89}Zr-J591 detected an additional 99 osseous sites. Forty-six lesions (21 bone and 25 soft tissue) were biopsied in 34 patients; 18 of 19 ^{89}Zr-J591–positive osseous sites and 14 of 16 ^{89}Zr-J591–positive soft tissue sites were positive for prostate cancer. The overall accuracy of ^{89}Zr-J591 was 95.2% (20 of 21) for osseous lesions and 60% (15 of 25) for soft-tissue lesions.

Conclusions: ^{89}Zr-J591 imaging demonstrated superior targeting of bone lesions relative to CIMs. Targeting soft-tissue lesions was less optimal, although ^{89}Zr-J591 had similar accuracy as individual CIMs. This study will provide benchmark data for comparing performance of proposed prostate-specific membrane antigen (PSMA) targeting agents for prostate cancer. *Clin Cancer Res; 21(23); 5277–85. ©2015 AACR.*

[1]Department of Radiology, Memorial Sloan Kettering Cancer Center, New York, New York. [2]Department of Radiology, Weill Cornell Medical College, New York, New York. [3]Department of Medical Physics, Memorial Sloan Kettering Cancer Center, New York, New York. [4]Molecular Pharmacology and Chemistry Program, Memorial Sloan Kettering Cancer Center, New York, New York. [5]Radiochemistry and Molecular Imaging Probe Core Facility, Memorial Sloan Kettering Cancer Center, New York, New York. [6]Department of Medicine, Memorial Sloan Kettering Cancer Center, New York, New York. [7]Department of Biostatistics, Memorial Sloan Kettering Cancer Center, New York, New York. [8]Department of Pathology, Dana-Farber Cancer Institute; Brigham & Women's Hospital; and Broad Institute, Boston, Massachusetts. [9]Department of Medicine, Weill Cornell Medical College, New York, New York. [10]Department of Pathology, Memorial Sloan Kettering Cancer Center, New York, New York. [11]Department of Surgery, Memorial Sloan Kettering Cancer Center, New York, New York.

Note: Supplementary data for this article are available at Clinical Cancer Research Online (http://clincancerres.aacrjournals.org/).

S.M. Larson and M.J. Morris share senior authorship.

Corresponding Author: Neeta Pandit-Taskar, Molecular Imaging and Therapy Service, Department of Radiology, Memorial Sloan Kettering Cancer Center, 1275 York Avenue, Box 77, New York, NY 10065. Phone: 212-639-3046; Fax: 212-717-3268; E-mail: pandit-n@mskcc.org

doi: 10.1158/1078-0432.CCR-15-0552

Introduction

The lack of imaging methods to directly visualize metastatic prostate cancer poses a challenge to staging, prognostication, and assessing treatment response of men with metastatic disease. Bone scintigraphy, the most common standard imaging modality for the evaluation of bone metastasis, is highly sensitive; however, it is also very nonspecific. The methylenediphosphonate bone scan (MDP) demonstrates reactive bone deposition but not cancer itself. Because many benign conditions may simulate tumor and therapeutic changes are not detectable early, and as regression and progression are indistinguishable, the practical use of MDP is somewhat limited. In addition, bone lesions as seen on computerized tomography (CT) and plain radiographs generally appear as sclerotic lesions and are unrelated to active tumor size; CT scans also cannot differentiate between the healing effects of therapy versus osteoblastic activity due to true disease progression. ^{18}F-flourodeoxyglucose (FDG) PET imaging, while it reflects increased glucose metabolism of more aggressive disease in patients with prostate cancer, has low sensitivity (1–6).

Accurate imaging modalities are therefore needed to develop imaging biomarkers, whether used for prognosis, prediction, or as surrogates for clinical effects. In addition, without the ability to

Translational Relevance

An imaging biomarker that accurately detects active metastatic disease, particularly in bone, will likely play a critical role in the management of advanced prostate cancer and selection of patients for optimal therapy. We studied ^{89}Zr-J591, a radiolabeled antibody targeting prostate-specific membrane antigen (PSMA) using PET imaging, and showed superior targeting of bone lesions relative to any standard imaging modality or combination of standard imaging modalities. This study establishes a benchmark to assess the effectiveness of alternative prostate cancer imaging biomarkers, including those targeting PSMA, such as radiolabeled minibody (IAB2M) or urea-based small peptides.

image the cancer directly, the acquisition of metastatic tissue for study and diagnostic purposes is impeded.

To overcome these limitations, we are developing an imaging biomarker for prostate cancer that is tumor-directed and quantifiable. Prostate-specific membrane antigen (PSMA) is a peptidase widely expressed by primary and metastatic prostate cancer (7, 8). Several imaging probes based on intact PSMA antibodies, antibody fragments, and small-molecule PSMA inhibitors have shown great promise for imaging prostate cancer with single-photon emission computed tomography (SPECT) and PET (9–25). While a number of other tracers have been used for assessment of disease in prostate cancer, thus far none have been validated in controlled clinical trials for routine clinical use (9–16).

A humanized monoclonal antibody huJ591 (J591) targets the extracellular domain of PSMA (17–20). Imaging of metastatic disease with ^{111}In-J591 and ^{177}Lu-J591 in prostate cancer and other tumors has been reported (21–24). More recently, we have developed and characterized ^{89}Zr-DFO-huJ591 (^{89}Zr-J591); ref. 25) for PET imaging of PSMA-expressing cancers. We conducted a first-in-human study of ^{89}Zr-J591 in metastatic prostate cancer and have previously reported on the safety, biodistribution, and pharmacokinetics of imaging with ^{89}Zr-J591 in patients with prostate cancer (21, 26). This study is an assessment of ^{89}Zr-J591 as an imaging biomarker and represents the analytic validation of the biomarker, as it assesses the performance characteristics of the tracer, using standard imaging modalities and biopsy specimens as comparators.

Materials and Methods

This was a phase I/II prospective study of ^{89}Zr-J591 in metastatic castration-resistant prostate cancer (mCRPC). The primary endpoints were to determine the safety, biodistribution, and tumor localization of ^{89}Zr-J591. Secondarily, it compared ^{89}Zr-J591 PET lesion detection with that of conventional imaging and tissue biopsies. Patients with progressive, histologically confirmed prostate cancer were eligible. Progression was defined as a new lesion on bone scan or an increase in measurable soft-tissue disease or new sites of soft-tissue disease detected by CT scan or MRI. Biochemical progression was defined as a minimum of 3 increasing PSA values from baseline with a minimum percentage increase of 25%. Additional eligibility criteria included a performance status of 60 or higher on the Karnofsky Performance Status (KPS) and adequate hepatic function. All patients underwent FDG-PET within 2 weeks and MDP and CT scan within 4 weeks before ^{89}Zr-J591 imaging. Patients with PSMA-positive cancers underwent no screening.

Antibody injection

The J591 was chelated with desferrioxamine-p-SCN (DFO) and subsequently radiolabeled with ^{89}Zr, using previously described methodology (27) and as detailed in our prior publication (26). The mean activity administered was 5.5.1 $\pm$ 0.4 mCi, and the mean amount of the radiolabeled J591 administered was 1.7 mg. All injections were coadministered with cold huJ591 antibody for a total antibody dose of 25 mg; this dose was chosen on the basis of prior studies that showed saturation of liver at 25-mg dose (23). The cold antibody was delivered intravenously over 5 minutes, followed immediately by a 1-minute infusion of the radiolabeled antibody. No premedications were administered to initial patients; however, because of minor grade I reactions of chills or rigors seen in a small number of patients, subsequent patients ($n = 15$) were premedicated with acetaminophen (500 mg) and Benadryl (25 mg).

PET imaging

Patients underwent PET scans extending from vertex to mid-thighs. In patients where skeletal disease in lower limbs was known to be present per conventional imaging, the scan was extended to include the thighs and entire legs. Four scans were performed on the first 10 patients at the following time points: 2–4 hours on the day of infusion, ~24 hours, 48–120 hours, and 144–168 hours. The remaining 40 patients were imaged 6 to 8 days after the antibody injection, based on the initial analysis indicating the best target-to-background ratios at that time point. All scans were performed on the same scanner (GE Discovery DSTE) in 3-dimensional mode with 7 min/FOV at days 6 to 8. Images were constructed using iterative reconstruction and attenuation correction.

Image interpretation and lesion detection

Lesion uptake with ^{89}Zr-J591 was evaluated using the last imaging time days 6 to 8 for all 50 patients. For each patient, whole-body images were visually and semiquantitatively analyzed. Foci of increased uptake were graded on a scale of 1–5 (1, negative; 2, probably negative; 3, equivocal; 4, probably positive; 5, definitely positive). Lesions graded 4 and 5 were considered positive. Equivocal uptake was further classified as positive or negative by consensus of 3 nuclear medicine readers (N. Pandit-Taskar, J.A. Carrasquillo, and S.M. Larson). Intensity of uptake was quantified by maximum standardized uptake values (SUVmax) for multiple lesions in a patient. Baseline FDG, CT scans, and ^{99m}Tc-MDP bone scans were reviewed for lesions by nuclear medicine physicians and radiologists who were blinded to the other imaging results. All lesions detected by each modality were recorded separately.

Lesion biopsy

Up to 2 lesions (one bone and one soft-tissue lesion, wherever feasible) were biopsied in patients who consented to biopsy, obtained within 4 weeks following ^{89}Zr-J591 imaging. The lesions most preferred for biopsy were those that had uptake on ^{89}Zr-J591 imaging or suspicious on all or most imaging modalities. The final

biopsy site was decided in consultation with the Interventional Radiology service for feasibility.

Image analysis

We implemented an analysis plan comprising 4 elements: (i) All detectable sites of disease by all modalities were graded by separate readers; (ii) each detectable lesion site on ^{89}Zr-J591 imaging was compared with standard imaging on a site-by-site basis, including ^{99m}Tc bone scan for bone lesions and CT scanning (limited cases with MRI as described in methods) for soft-tissue lesions; (iii) Pathology of image-directed biopsy tissue sites was compared with imaging findings; and (iv) for all non-biopsied sites of ^{89}Zr-J591 imaging, follow-up imaging performed for clinical reasons was evaluated to determine the presence or absence of disease at the site of uptake.

The concordance between ^{89}Zr-J591 and MDP was determined by plotting the number of lesions detected by ^{89}Zr-J591 scan versus MDP for each of the 50 patients.

Statistical analysis

This prospective study was designed with the objective of evaluating the ability of ^{89}Zr-J591 to detect known sites of disease. Because no gold standard is available, a known site of disease was defined in the protocol as any lesion that was identified by conventional imaging methods at baseline. This does not lend itself to accurate estimation of specificity, so the protocol focused on the estimation of sensitivity using all sites identified by conventional imaging as the denominator. Assuming an intrapatient correlation of 0.1 (based on our experience of FDG-PET in this disease), the estimate of sensitivity was projected to be within $\pm$9% of its true value if we accrued 50 patients, assuming that the true sensitivity is 50%. If the sensitivity is higher, then our estimates will be more precise. Soft-tissue lesions and bone lesions were treated separately.

We also used an emerging methodology to predict the number of positive lesions among the nonbiopsied sites based on information from the biopsied sites. The details of this method are provided in the Appendix. Briefly, this method considers the information from the biopsied sites as prior (represented by a β distribution) and derives a posterior distribution using the Bayes theorem. The number of positive lesions among the nonbiopsied sites is calculated from the implied β-binomial distribution.

Results

Patients

A total of 50 patients with progressive mCRPC were studied prospectively (Supplementary Table S1). The protocol was approved by the Institutional Review Board of Memorial Sloan Kettering Cancer Center (New York, NY), the sole study site, and all patients provided signed informed consent. All patients underwent CT scan of chest, abdomen, and pelvis, as well as bone scintigraphy (MDP) within a month before imaging with ^{89}Zr-J591. In addition, all patients received an FDG-PET/CT scan within 2 weeks before ^{89}Zr-J591 imaging. In 2 patients, an MRI of abdomen and pelvis was performed for clinical reasons and used for comparison of soft-tissue findings (lesion in liver and a retroperitoneal node) and an additional 2 patients received a clinical MRI of the spine and femur, which was used for confirmation of bone lesion findings.

Administration of ^{89}Zr-J591 antibody was associated with infusion reactions in 16 patients, none of whom were premedicated. The reactions included grade I chills ($n = 12$) and grade I chills with rigors ($n = 4$). Three patients reported heavy breathing or shortness of breath and were treated with Benadryl 50 mg intravenously. In 2 of these patients, additional hydrocortisone 50 mg intravenously was administered. This is similar to our prior experience with the antibody (22, 23, 28, 29). No side effects were noted in patients who were premedicated.

Patient-based analysis

The distribution of lesions across bone, lymph nodes, and viscera are described in Supplementary Table S1. ^{89}Zr-J591 antibody scans were positive in 44 of 50 patients for either bone and/or soft-tissue lesions. Osseous lesions were seen in 29 of 50 patients with ^{89}Zr-J591as compared with 27 of 50 for bone scans. Visceral/nodal disease was seen in 27 of 50 patients with ^{89}Zr-J591as compared with 31 of 50 for CT scans. Of the 6 patients with negative ^{89}Zr-J591 scans, 4 had soft tissue or nodal disease seen on CT or FDG and 2 of 6 patients had bone lesions seen on MDP.

Analysis of bone lesions

A total of 439 lesions were detected by conventional imaging modalities, 392 of which were seen on ^{89}Zr-J591 (Table 1, Supplementary Fig. S2), resulting in a sensitivity of 89% [95% confidence interval (CI), 85.5%–93.5%]. These calculations follow the protocol definition of sensitivity and are also adjusted for clustering. MDP detected 339 lesions, whereas ^{89}Zr-J591 detected 491 sites. Of these, 302 sites were detected by both MDP and ^{89}Zr-J591 (89% concordance). ^{89}Zr-J591 showed 189 additional lesions in 23 patients that were not detected by MDP. MDP detected 37 lesions that were not detected by ^{89}Zr-J591 imaging. There was a linear relationship for the number of lesions detected by ^{89}Zr-J591scan versus MDP (Supplementary Fig. S1), with an estimated 34% higher detection rate for ^{89}Zr-J591 scan0-positive lesions, across all of the patients. A total of 99 lesions were detected by ^{89}Zr-J591 imaging alone that were not seen by any other modality.

Table 1. Bone and soft-tissue lesions

	Bone lesions								
	MDP$^+$	MDP$^-$	FDG$^+$	FDG$^-$	CT$^+$	CT$^-$	CIM$^+$	CIM$^-$	Total
Zr-J591$^+$	302	189	202	289	281	210	392	99	491
Zr-J591$^-$	37	10	5	42	20	27	47	NA	
Total	339	199	207	331	301	237	439	99	

	Soft-tissue lesions						
	FDG$^+$	FDG$^-$	CT$^+$	CT$^-$	CIM$^+$	CIM$^-$	Total
Zr-J591$^+$	43	47	65	25	73	17	90
Zr-J591$^-$	45	29	59	15	74	NA	
Total	88	76	124	40	147	17	

NOTE: Comparative lesion detection by imaging modality.

Lesions detected on ^{89}Zr-J591 imaging but not on MDP (J591^{+}/MDP^{-}). There were 189 ^{89}Zr-J591^{+}/MDP^{-} lesions. Of these, 49 were also seen on FDG, another 35 showed stable sclerotic lesions on CT, and 64 other lesions were positive on follow-up MDP or FDG (obtained 1 to 6 months later with a median time of 4 months; Fig. 1 and Supplementary Fig. S2). There were 41 lesions that were not confirmed to be metastatic prostate cancer within a follow-up time of 6 months; the impact of post-study treatment is unknown.

Lesions detected on MDP but not on ^{89}Zr-J591 imaging (J591^{-}/MDP^{+}). A total of 37 sites were seen on MDP but not on ^{89}Zr-J591. Of these, 35 sites were also FDG-negative, whereas 2 were FDG-positive. The latter 2 sites (MDP-positive, FDG-positive, and ^{89}Zr-J591–negative) were biopsied and found to be negative for metastatic prostate cancer on histopathology (Fig. 2). Of the 37 sites, 20 represented known sites of metastasis in correlation with other prior imaging with stable sclerosis on CT and exhibited increased uptake in the follow-up bone scan. An additional 8 of 37 sites were found to have benign etiology on follow-up imaging, whereas 9 of 37 remained stable on MDP and negative on FDG follow-up imaging.

Analysis of soft tissue

A total of 147 soft-tissue lesions were identified by conventional imaging modalities, 73 of which were seen on ^{89}Zr-J591, resulting in a sensitivity of 50% (95% CI, 39–61). ^{89}Zr-J591 imaging detected 90 soft-tissue lesions in comparison to 124 soft-tissue lesions detected by CT (Table 1). The lesions primarily included nodes; other soft tissue and organs included

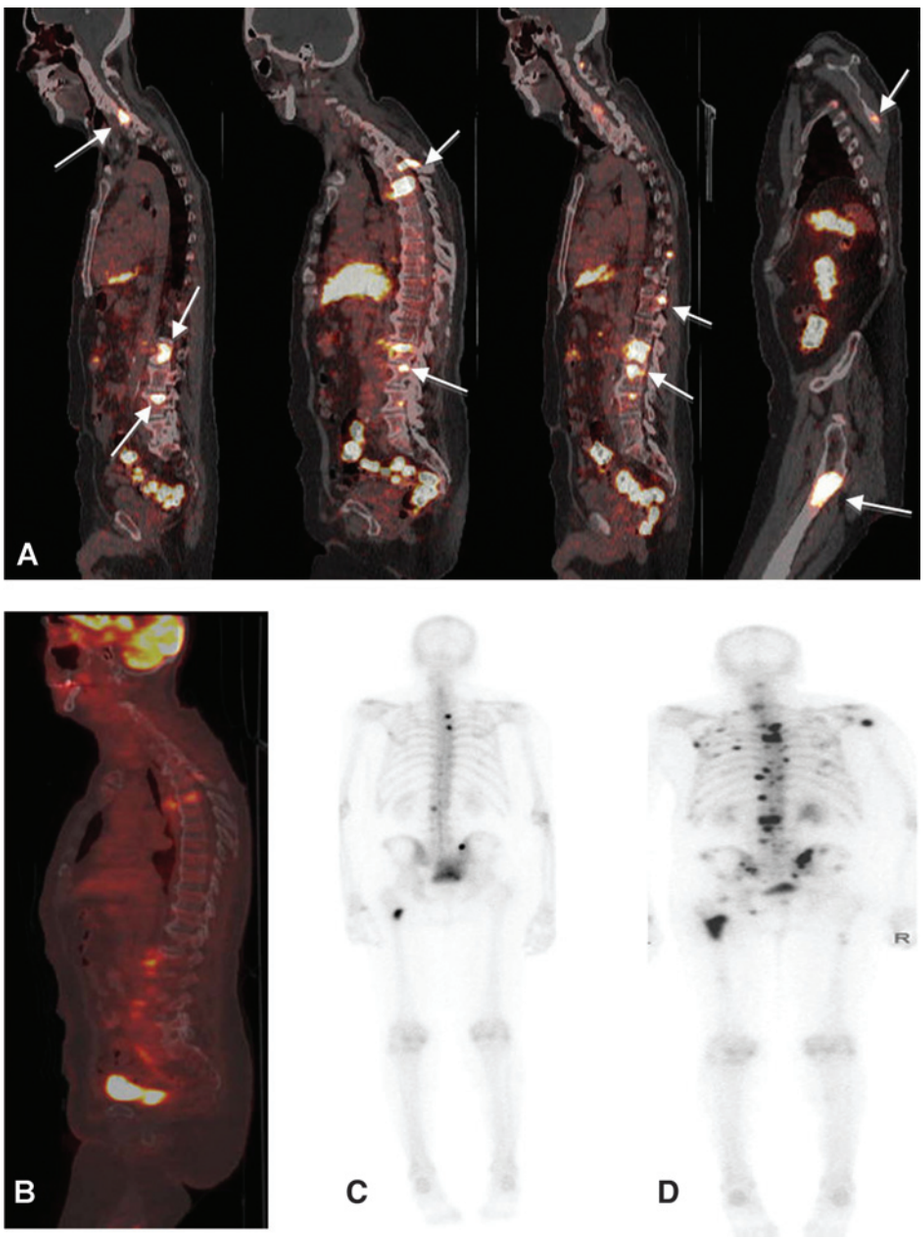

Figure 1.
Patient with metastatic prostate cancer (PSA 90.9) with ^{89}Zr-J591-positive lesions that were not seen on MDP. Follow-up imaging showed POD on MDP. ^{89}Zr-J591 scan (A) showed uptake in multiple bone sites (arrows) that were not seen on concurrent FDG scan (B) or bone scan (C). A follow-up bone scan (D) showed uptake in the sites and was consistent with POD.

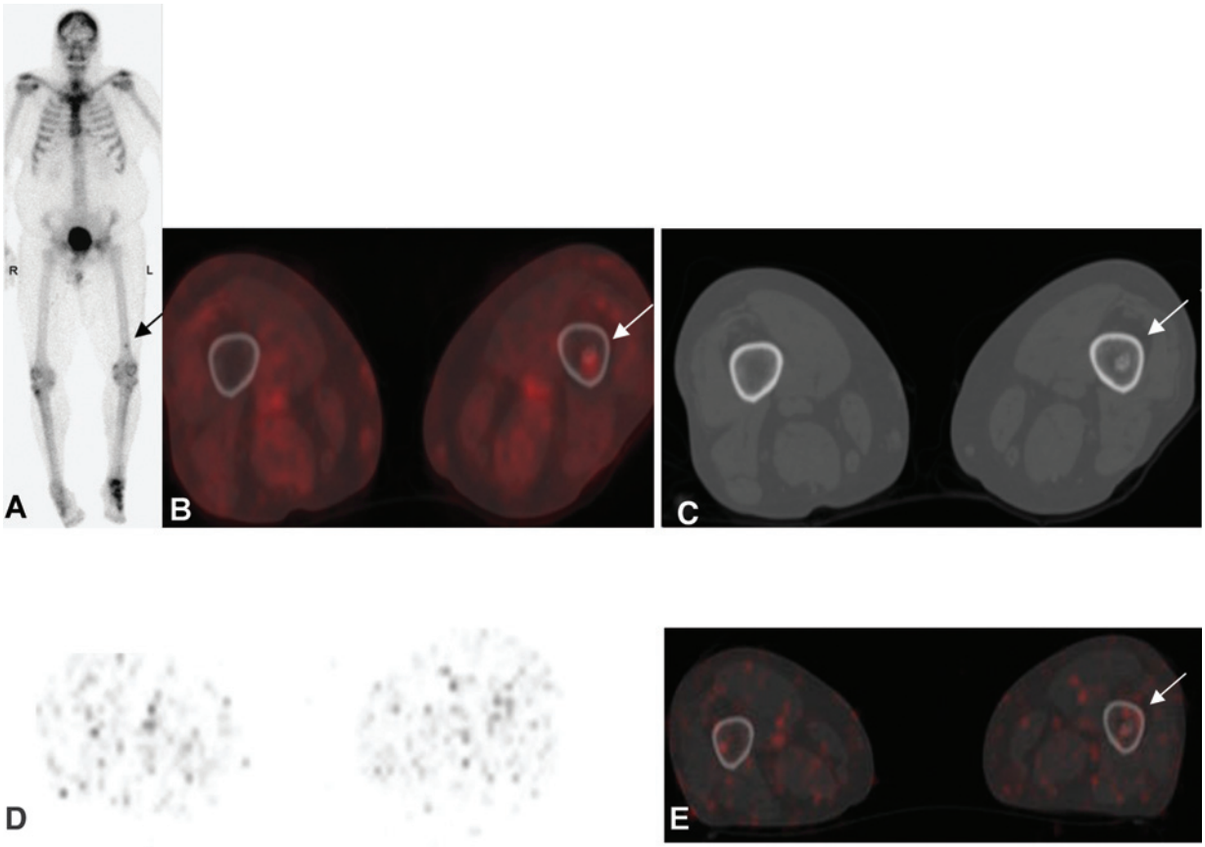

Figure 2.
Patient with metastatic prostate cancer (PSA of 27.4). Baseline bone scan (A) and FDG-PET (B) showed suspicious uptake in left femur distally (arrow); CT scan (C) showed sclerotic focus in the region. ^{89}Zr-J591 scan transaxial and fused images (D and E) did not show any suspicious uptake. Biopsy of the femoral lesion showed benign enchondroma.

lung (n = 12), prostate bed (n = 4), liver (n = 3), adrenal (n = 2), seminal vesicle (n = 2), posterior bladder wall (n = 1), and brain lesion (n = 1). There were 65 (52%) concordant ^{89}Zr-J591 and CT-positive lesions; ^{89}Zr-J591 identified an additional 25 lesions (20%) not detected by CT scan but was negative for 59 lesions detected by CT.

There were 43 concordant lesions between FDG and ^{89}Zr-J591, whereas ^{89}Zr-J591 identified an additional 47 lesions not detected by FDG. ^{89}Zr-J591 did not identify 45 lesions that were positive on FDG. These lesions were predominantly mediastinal lymph nodes and lung nodules. Most of these lesions were sub-centimeter in size measuring 0.5 to 0.8 mm; 2 nodes measured 1.1 and 2.1 cm, and were close to the vasculature in the subaortic region or hilum. A total of 147 soft-tissue lesions were seen by combined CT and FDG-PET/CT imaging. In comparison to combined CT and FDG, ^{89}Zr-J591 showed 17 additional sites of disease.

Biopsy assessment

A total of 22 osseous sites (21 evaluable) and 25 soft tissue sites were biopsied in 34 patients.

Bone lesions. There were 21 evaluable osseous sites; 19 were ^{89}Zr-J591–positive, whereas 2 sites were negative on ^{89}Zr-J591 imaging

Table 2. Biopsy correlation with imaging

	J591$^+$	J591$^-$	MDP$^+$	MDP$^-$	FDG$^+$	FDG$^-$
Bone lesions						
Biopsy-positive (n = 18)	18[a]	0	14	4	14	4
Biopsy-negative (n = 3)	1	2	1	2	2	1
Soft-tissue lesions						
Biopsy-positive (n = 22)	14	8	18	4	13	9
Biopsy-negative (n = 3)	2	1	1	2	2	1

[a]One site was originally negative on pathology but showed progression on follow-up imaging; a repeat biopsy (performed clinically) was positive for metastatic disease.

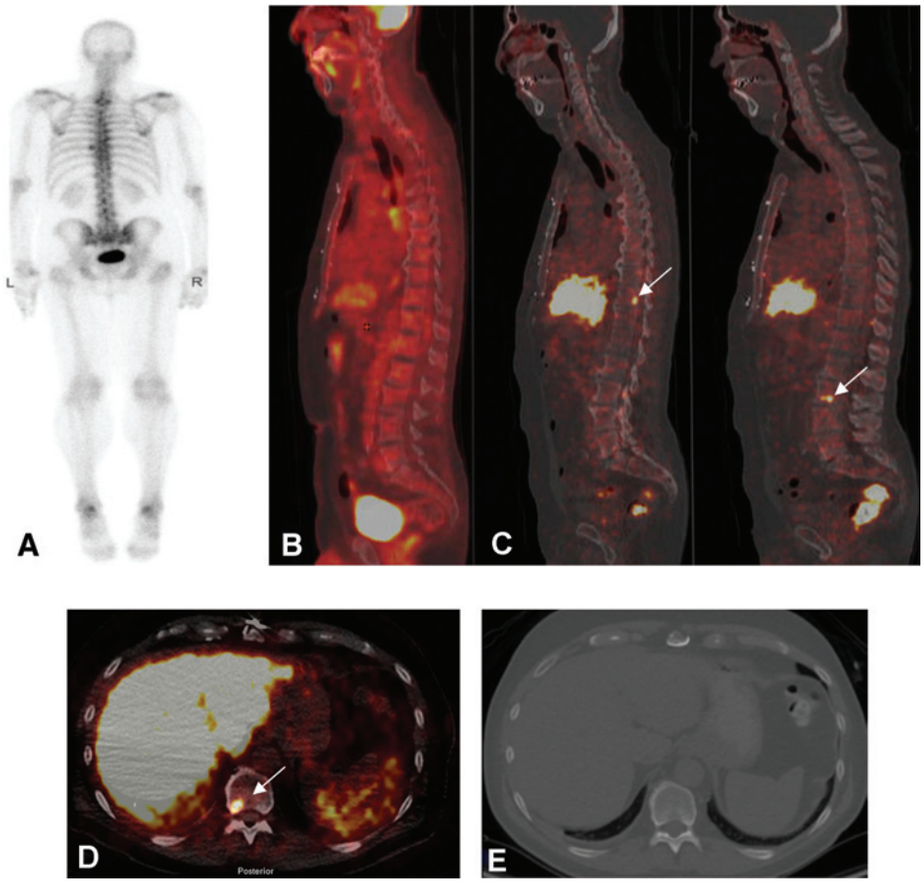

Figure 3.
Patient with metastatic prostate cancer (PSA of 4.1). Baseline bone scan (A) and FDG-PET (B) showed no suspicious lesions. ^{89}Zr-J591 scan (C) showed uptake in T11 and L3 as seen on sagittal images (C) and transaxial image (D; arrows). CT scan did not show any corresponding abnormality (E). Biopsy of T11 was positive for metastatic carcinoma.

but had uptake on FDG-PET (Table 2). Overall, 17 of 19 ^{89}Zr-J591–positive sites were also positive on pathology, whereas 2 sites were negative on pathology. One of these pathology-negative sites showed metastatic disease on MRI and a repeat biopsy performed clinically was positive for disease at this site. Thus, 18 of 19 (95%) osseous sites visible on ^{89}Zr-J591 PET imaging were considered true positives; 4 of these were seen only on ^{89}Zr-J591 imaging and had no correlate on other concurrent imaging modalities. Accordingly, 4 sites of occult disease were considered confirmed in bone (Fig. 3). Two of the ^{89}Zr-J591–negative sites were biopsied; both were also negative for malignancy on pathology and follow-up. The overall accuracy in the biopsied osseous sites was 95.2% (21 of 22).

Soft-tissue lesions. A total of 25 soft-tissue lesions were biopsied, 22 of which were positive on pathology (Table 2). Of these 22, 14 ^{89}Zr-J591–positive (64%) and 8 ^{89}Zr-J591–negative sites (36%) were positive on pathology. CT was positive in 18 of 22 (84%) and FDG was positive in 13 of 22 (59%) of the biopsy-proven malignant lesions. There were 2 lesions that were positive on ^{89}Zr-J591 PET/CT but negative on pathology: one of these was adrenal gland uptake that was not suspicious on FDG and CT scan and was not positive on follow-up, whereas the second site was an external iliac node, which was also suspicious by FDG-PET and CT scan. However, this site was benign on pathology and stable in FDG uptake and size on follow-up.

^{89}Zr-J591 imaging was negative for 8 of 22 pathologic positive sites, whereas FDG was negative for 9 of 22 sites. These 8 of 22 lesions were considered false-negatives for ^{89}Zr-J591 imaging and included nodes, liver, and lung lesions that were otherwise seen on CT or FDG scan.

^{89}Zr-J591 lesion uptake: SUV comparison of bone and soft-tissue lesions

Uptake was higher overall in the bone lesions than in the soft-tissue lesions. The maximum SUV normalized for body weight (SUVmaxbw) for the bone lesions ranged from 1.35 to 37.2 with a median of 8.9. The SUVmaxbw for the nodal lesions ranged from 1.67 to 18.31 (median, 4.8) and between 1.0 and 30.46 (median, 4.8) for other soft-tissue lesions. The difference between the SUVmax of bone lesions and all soft-tissue lesions, including visceral and nodal disease, was statistically significant ($P < 0.001$). A comparison of SUV for soft tissue versus bone lesions within the same patient indicated that the uptake in bone lesions was independent of the uptake in soft-tissue lesions, with no correlation observed. The SUV was independent of lesion size, and the number of soft tissue or bone lesions in a patient was independent of each other, with no correlation seen in intrapatient analysis.

^{89}Zr-J591 lesion detection and PSA levels

The overall PSA range for these patients was 0.05 to 1,374 ng/mL (one patient had PSA of 1,374.6; otherwise, the

maximum PSA level was 115.6 ng/mL). ^{89}Zr-J591 detected lesions in a patient with PSA as low as 0.23 ng/mL; in this patient, 2 bone lesions were detected, of which one was biopsy-proven for metastatic prostate disease. ^{89}Zr-J591 showed lesions in 6 of 8 patients with PSA < 1 ng/mL (2 with bone lesions, 3 with nodal disease, and 1 with both soft tissue and bone lesions; see Supplementary Fig. S3) and an additional 10 of 11 patients with PSA below 2.5 ng/mL (6 with soft-tissue lesions, 3 with bone lesions, and 1 with both bone and soft-tissue lesions).

Predicted number of positive lesions among nonbiopsied sites

We observed 439 bone and 147 soft-tissue lesions with conventional imaging, providing precisions of ±3.5% and 11.5%, respectively, using the value of 0.1 for intraclass correlation. Using an emerging method of Bayesian analysis, we predicted the number of positive lesions among the nonbiopsied sites for each modality separately for bone and soft tissue. The results, shown in Table 3, indicate that ^{89}Zr-J591 ranks the highest among all modalities in osseous tissue in terms of predicted number of positive findings (425, 95% posterior interval, 352–465), followed by bone scan (281, 220–314), CT (233, 176–270), and FDG (155, 116–180). In soft-tissue lesions, CT had the highest number of predicted positives (86, 67–97), followed by ^{89}Zr-J591 (54, 40–64) and FDG (52, 37–61).

Discussion

This is the first-in-human prospective phase I/II analytic validation study of a well-characterized anti-PSMA antibody (J591) that uses ^{89}Zr-J591 PET for imaging metastatic prostate cancer. For comparators, we used a lesion multimodality imaging comparison and biopsy data. We have previously reported the safety and biodistribution of ^{89}Zr-J591 in the first 10 patients in this cohort (26) and identified the optimal time for imaging with this intact antibody to be between days 6 and 8. We expanded the cohort to include an additional 40 patients with mCRPC to assess the ability of ^{89}Zr-J591 to accurately detect bone and soft tissue involvement in mCRPC. To our knowledge, this is the first comprehensive evaluation of anti-PSMA PET imaging in correlation with conventional imaging to evaluate its role as a biomarker.

^{89}Zr-J591 PET was superior for detecting bone metastases and bone lesions that were occult by the conventional imaging modalities of MDP, CT, and FDG. ^{89}Zr-J591 identified significantly more lesions than MDP, the most common modality for detecting bone metastasis in prostate cancer. In addition, ^{89}Zr-J591 scans detected more skeletal lesions than FDG-PET alone and combined findings on conventional imaging (Fig. 3). A post-hoc analysis with follow-up imaging showed that about 75% of the additional lesions detected by ^{89}Zr-J591 subsequently became MDP-positive at the same site and about 19% had stable sclerosis on CT scan. These findings suggest that ^{89}Zr-J591 targets PSMA expression in viable disease that was not detected initially (MDP) or appeared stable (CT). The limitation of this interpretation is the assumption that a lesion seen in more than one modality is probably true disease. The visualization of the same sites on other imaging modalities at a later time may represent progression or, perhaps more likely, a difference in the ability to detect disease. We concluded that ^{89}Zr-J591imaging is able to detect viable disease earlier than conventional imaging. For lesions that were not initially seen on ^{89}Zr-J591 imaging compared to bone scan, most were nonhypermetabolic by FDG imaging with stable sclerosis on CT (site correlated). These tumor sites may represent inactive or treated disease.

Our study also confirmed ^{89}Zr-J591–positive sites by pathology to verify the finding of ^{89}Zr-J591 lesion uptake on a site-by-site basis, a critical component of this analysis. There was an overall high accuracy of ^{89}Zr-J591 lesion detection in correlation with pathology for bone metastasis. Although biopsy confirmation is ideal for establishing the presence of disease, there is a practical limitation of biopsying every (and sometimes, any) lesion seen on ^{89}Zr-J591 imaging. Because a majority of ^{89}Zr-J591–positive bony lesions were pathologically proven malignant, projections using Bayes' rule suggest that a large number (427 of 472) of nonbiopsied bony sites are also likely true-positive sites, which would imply that the 170 of 189 additional sites seen by ^{89}Zr-J591 compared with MDP would be projected to be metastatic disease, as would 89 of 99 of the occult sites seen by ^{89}Zr-J591 compared with conventional imaging. This suggests that ^{89}Zr-J591 can likely detect occult sites of disease in advanced prostate cancer that otherwise went undetected—in this series, 50% more bone lesions than were detected by bone scan.

On the basis of the imaging analysis, biopsy results, and statistical projections, we conclude that ^{89}Zr-J591–targeted imaging of PSMA is highly sensitive and accurate for bone disease with ≥90% probability that positive lesions are likely to represent true prostate cancer. In contrast, ^{89}Zr-J591 performed less well for the detection of soft-tissue lesions, with an overall accuracy of 60%. ^{89}Zr-J591 PET in soft tissue sites clearly had lower uptake, with SUVmax < 50% of bone SUVs and highly variable performance in soft-tissue lesions overall. The detection of soft-tissue lesions by ^{89}Zr-J591 (50% concordance with CIMs) was, however, similar to FDG imaging (47%). Few false-positive soft-tissue lesions were detected by ^{89}Zr-J591, suggesting high specificity.

Table 3. Bayesian prediction for disease in visualized lesions

Modality	Tissue	Sites + on scans	Total sites biopsied	Total pathology + lesions	Number of scan + sites biopsied	Scan+ and biopsy+	Nonbiopsied, scan + sites	Estimated biopsy + sites of nonbiopsied scan + group	95% CI
J591	Bone	491	21	18[a]	19	18[a]	470	425	352–465
BS	Bone	339	21	18[a]	15	14	318	281	220–314
CT	Bone	301	21	18[a]	16	14	280	233	176–270
FDG	Bone	207	21	18[a]	16	14	186	155	116–180
CT	Soft	124	25	22	20	18	99	86	67–97
J591	Soft	90	25	22	16	14	65	54	40–64
FDG	Soft	88	25	22	15	13	63	52	37–61

[a]One site was originally negative on pathology but showed progression on follow-up imaging; a repeat biopsy (performed clinically) was positive for metastatic disease.

The lower detection rate of soft tissue disease may relate to generalized lower uptake. In addition, the proximity of nodal lesions to vasculature, which retains activity for several days, limits the evaluation of nodal disease. Furthermore, other benign etiologies such as inflammation or granulomatous disease that were presumed as disease on CT and FDG scan may contribute to higher false-negative numbers noted for ^{89}Zr-J591. It is possible that the size of the intact antibody itself slows intratumoral penetration and may interfere with antibody binding and uptake in soft tissue metastases or that the PSMA expression itself is lower in soft tissue disease than osseous metastases. Detailed molecular analysis is underway to evaluate these possibilities. The exact reason for overall lower uptake and detection of soft-tissue lesions is not known at this time.

We recognize certain limitations of the study, as well as potential for bias. Most importantly, there is no single test that can serve as a gold standard for comparison. This constrains the assessment of the absolute total number of true lesions in a given patient. While a biopsy of every lesion is not practically possible given widespread skeletal disease in many patients, targeting the positive lesion introduces a bias toward assessment of the positive site only. In addition, lesion detection may be limited by size and system resolution. For smaller lesions, about 250 mg in volume or less must have a substantial uptake of 5:1 to actually be seen (30). The treatment received by patients following the imaging was variable, which limited the assessment of lesions through follow-up imaging.

^{89}Zr-J591 PET imaging also presents some practical limitations. Because of the larger size of the antibody leading to the long blood clearance time, 6 to 8 days are required for optimal tumor visualization, postinjection. The hepatic and renal uptake is considerable, which interferes with the detection of rare metastases to these organs. Dosimetry to these organs limits the dose of injected activity and later imaging requires longer duration. The assessment of soft tissue disease appears less optimal. Given these limitations, smaller molecular agents directed to PSMA that have faster clearance and show lesions earlier may be more suitable for assessment. We are now exploring the use of an anti-PSMA minibody derived from J591 (31) for the detection of early changes in bone disease in advanced prostate cancer and assessment of treatment response in castration-resistant prostate cancer.

Disclosure of Potential Conflicts of Interest

S.B. Solomon reports receiving a commercial research grant from GE Healthcare. N.H. Bander has ownership interest (including patents) in and is a consultant/advisory board member for BZL Biologics, LLC. S.M. Larson reports receiving commercial research support from ImaginAb, Genentech, and Regeneron, and is a consultant/advisory board member for Jansson, Merck, and Progenics. M.J. Morris reports receiving commercial research support from Exini and ImaginAb, and speakers bureau honoraria from Fujifilm. No potential conflicts of interest were disclosed by the other authors.

Authors' Contributions

Conception and design: N. Pandit-Taskar, J.A. O'Donoghue, S.K. Lyashchenko, J.A. Carrasquillo, M. Gönen, M. Loda, J.R. Osborne, J.S. Lewis, N.H. Bander, H.I. Scher, S.M. Larson, M.J. Morris

Development of methodology: N. Pandit-Taskar, J.A. O'Donoghue, S.K. Lyashchenko, S.M. Cheal, V. Beylergil, J.A. Carrasquillo, M. Loda, N.H. Bander, H.I. Scher, S.M. Larson, M.J. Morris

Acquisition of data (provided animals, acquired and managed patients, provided facilities, etc.): N. Pandit-Taskar, J.A. O'Donoghue, J.C. Durack, S.M. Cheal, V. Beylergil, R.A. Lefkowitz, J.A. Carrasquillo, D.F. Martinez, A.M. Fung, S.B. Solomon, M. Loda, D.M. Nanus, S.T. Tagawa, V.E. Reuter, H.I. Scher, S.M. Larson, M.J. Morris

Analysis and interpretation of data (e.g., statistical analysis, biostatistics, computational analysis): N. Pandit-Taskar, J.A. O'Donoghue, V. Beylergil, R.A. Lefkowitz, J.A. Carrasquillo, D.F. Martinez, S.B. Solomon, M. Gönen, G. Heller, M. Loda, W.A. Weber, N.H. Bander, H.I. Scher, S.M. Larson, M.J. Morris

Writing, review, and/or revision of the manuscript: N. Pandit-Taskar, J.A. O'Donoghue, J.C. Durack, V. Beylergil, R.A. Lefkowitz, J.A. Carrasquillo, D.F. Martinez, S.B. Solomon, M. Gönen, S.T. Tagawa, J.L. Feldman, J.S. Lewis, W.A. Weber, N.H. Bander, H.I. Scher, S.M. Larson, M.J. Morris

Administrative, technical, or material support (i.e., reporting or organizing data, constructing databases): N. Pandit-Taskar, V. Beylergil, J.A. Carrasquillo, D.F. Martinez, A.M. Fung, J.L. Feldman, J.R. Osborne, J.S. Lewis, H.I. Scher, S.M. Larson, M.J. Morris

Study supervision: N. Pandit-Taskar, J.A. Carrasquillo, D.F. Martinez, J.S. Lewis, S.M. Larson, M.J. Morris

Other (wrote the article, compiled the figures and tables, and reviewed the policies of AACR on data and image presentation): N. Pandit-Taskar

Other (PI of STARR grant that provided the bulk of the support for the project): S.M. Larson

Other (PI of the clinical trial): M.J. Morris

Acknowledgments

The authors thank the research study assistants, clinical research coordinators, research managers, research nurses, technologists, and radiopharmacists for making this study possible. The authors also thank Leah Bassity for her editorial assistance.

Grant Support

This study was funded by Starr Cancer Consortium, the prostate cancer program of Memorial Sloan Kettering Cancer Center, the Center for Targeted Radioimmunotherapy and Theranostics of the Ludwig Center for Cancer Immunotherapy, and the David H. Koch Foundation. In addition, the Radiochemistry & Molecular Imaging Probes Core of MSK is supported in part by NIH P30CA008748, the Landy Research Fund, and Hascoe Charitable Foundation.

The costs of publication of this article were defrayed in part by the payment of page charges. This article must therefore be hereby marked *advertisement* in accordance with 18 U.S.C. Section 1734 solely to indicate this fact.

Received March 6, 2015; revised May 20, 2015; accepted June 28, 2015; published OnlineFirst July 14, 2015.

References

1. Jadvar H, Desai B, Ji L, Conti PS, Dorff TB, Groshen SG, et al. Baseline 18F-FDG PET/CT parameters as imaging biomarkers of overall survival in castrate-resistant metastatic prostate cancer. J Nucl Med 2013;54:1195–201.
2. Yu EY, Muzi M, Hackenbracht JA, Rezvani BB, Link JM, Montgomery RB, et al. C11-acetate and F-18 FDG PET for men with prostate cancer bone metastases: relative findings and response to therapy. Clin Nucl Med 2011;36:192–8.
3. Sengoku T, Matsumura K, Usami M, Takahashi Y, Nakayama T. Diagnostic accuracy of FDG-PET cancer screening in asymptomatic individuals: use of record linkage from the Osaka Cancer Registry. Int J Clin Oncol 2014 19:989–97.
4. Minamimoto R, Uemura H, Sano F, Terao H, Nagashima Y, Yamanaka S, et al. The potential of FDG-PET/CT for detecting prostate cancer in patients with an elevated serum PSA level. Ann Nucl Med 2011;25:21–7.
5. Morris MJ, Akhurst T, Larson SM, Ditullio M, Chu E, Siedlecki K, et al. Fluorodeoxyglucose positron emission tomography as an outcome measure for castrate metastatic prostate cancer treated with antimicrotubule chemotherapy. Clin Cancer Res 2005;11:3210–6.
6. Meirelles GS, Schoder H, Ravizzini GC, Gonen M, Fox JJ, Humm J, et al. Prognostic value of baseline [18F] fluorodeoxyglucose positron emission tomography and 99mTc-MDP bone scan in progressing metastatic prostate cancer. Clin Cancer Res 2010;16:6093–9.

7. Murphy GP, Elgamal AA, Su SL, Bostwick DG, Holmes EH. Current evaluation of the tissue localization and diagnostic utility of prostate specific membrane antigen. Cancer 1998;83:2259–69.
8. Bostwick DG, Pacelli A, Blute M, Roche P, Murphy GP. Prostate specific membrane antigen expression in prostatic intraepithelial neoplasia and adenocarcinoma: a study of 184 cases. Cancer 1998;82: 2256–61.
9. McCarthy M, Siew T, Campbell A, Lenzo N, Spry N, Vivian J, et al. (1)(8)F-Fluoromethylcholine (FCH) PET imaging in patients with castration-resistant prostate cancer: prospective comparison with standard imaging. Eur J Nucl Med Mol Imaging 2011;38:14–22.
10. Ceci F, Castellucci P, Graziani T, Schiavina R, Brunocilla E, Mazzarotto R, et al. (11)C-Choline PET/CT detects the site of relapse in the majority of prostate cancer patients showing biochemical recurrence after EBRT. Eur J Nucl Med Mol Imaging 2014;41:878–86.
11. Picchio M, Spinapolice EG, Fallanca F, Crivellaro C, Giovacchini G, Gianolli L, et al. [11C]Choline PET/CT detection of bone metastases in patients with PSA progression after primary treatment for prostate cancer: comparison with bone scintigraphy. Eur J Nucl Med Mol Imaging 2012; 39:13–26.
12. Rodari M, Lopci E, Pepe G, Antunovic L, Chiti A. [11C]-choline PET/CT in imaging locally advanced prostate cancer. Nucl Med Rev Cent East Eur 2011;14:118–9.
13. Haseebuddin M, Dehdashti F, Siegel BA, Liu J, Roth EB, Nepple KG, et al. 11C-acetate PET/CT before radical prostatectomy: nodal staging and treatment failure prediction. J Nucl Med 2013;54:699–706.
14. Beheshti M, Imamovic L, Broinger G, Vali R, Waldenberger P, Stoiber F, et al. 18F choline PET/CT in the preoperative staging of prostate cancer in patients with intermediate or high risk of extracapsular disease: a prospective study of 130 patients. Radiology 2010;254:925–33.
15. Larson SM, Morris M, Gunther I, Beattie B, Humm JL, Akhurst TA, et al. Tumor localization of 16beta-18F-fluoro-5alpha-dihydrotestosterone versus 18F-FDG in patients with progressive, metastatic prostate cancer. J Nucl Med 2004;45:366–73.
16. Afshar-Oromieh A, Zechmann CM, Malcher A, Eder M, Eisenhut M, Linhart HG, et al. Comparison of PET imaging with a (68)Ga-labelled PSMA ligand and (18)F-choline-based PET/CT for the diagnosis of recurrent prostate cancer. Eur J Nucl Med Mol Imaging 2014;41:11–20.
17. Hamilton A, King S, Liu H, Moy P, Bander N, Carr F. A novel humanised antibody against prostate specific membrane antigen (PSMA) for in vivo targeting and therapy. Proc Am Assoc Cancer Res Ann Mtg 1998; 39:440.
18. Bander NH, Trabulsi EJ, Kostakoglu L, Yao D, Vallabhajosula S, Smith-Jones P, et al. Targeting metastatic prostate cancer with radiolabeled monoclonal antibody J591 to the extracellular domain of prostate specific membrane antigen. J Urol 2003;170:1717–21.
19. Bander NH, Nanus DM, Milowsky MI, Kostakoglu L, Vallabahajosula S, Goldsmith SJ. Targeted systemic therapy of prostate cancer with a monoclonal antibody to prostate-specific membrane antigen. Semin Oncol 2003;30:667–77.
20. Bander NH, Nanus D, Bremer S, Smith-Jones P, Kostakoglu L, Vallabhajosula S, et al. Phase 1 clinical trial targeting a monoclonal antibody (mAb) to the extracellular domain of prostate specific membrane antigen (PSMAext) in hormone-independent patients. J Urol 2000;163(4 Suppl): 160.
21. Pandit-Taskar N, O'Donoghue JA, Morris MJ, Wills EA, Schwartz LH, Gonen M, et al. Antibody mass escalation study in patients with castration-resistant prostate cancer using (111)In-J591: lesion detectability and dosimetric projections for (90)Y Radioimmunotherapy. J Nucl Med 2008;49:1066–74.
22. Morris MJ, Pandit-Taskar N, Divgi CR, Bender S, O'Donoghue JA, Nacca A, et al. Phase I evaluation of J591 as a vascular targeting agent in progressive solid tumors. Clin Cancer Res 2007;13:2707–13.
23. Morris MJ, Divgi CR, Pandit-Taskar N, Batraki M, Warren N, Nacca A, et al. Pilot trial of unlabeled and indium-111-labeled anti-prostate-specific membrane antigen antibody J591 for castrate metastatic prostate cancer. Clin Cancer Res 2005;11:7454–61.
24. Vallabhajosula S, Kostakoglu L, Hamacher KA, Brandman S, Bander NH, Goldsmith SJ. Pharmacokinetics, biodistribution and radiation dosimetry of radiolabeled anti-PSMA antibody: comparison of In-111-DOTA-J591 with Lu-177-dota-J591. J Nucl Med 2003;44:322P-P.
25. Holland JP, Divilov V, Bander NH, Smith-Jones PM, Larson SM, Lewis JS. Zr-89-DFO-J591 for immunoPET of prostate-specific membrane antigen expression in vivo. J Nucl Med 2010;51:1293–300.
26. Pandit-Taskar N, O'Donoghue JA, Beylergil V, Lyashchenko S, Ruan S, Solomon SB, et al. 89Zr-huJ591 immuno-PET imaging in patients with advanced metastatic prostate cancer. Eur J Nucl Med Mol Imaging 2014; 41:2093–105.
27. Vosjan MJ, Perk LR, Visser GW, Budde M, Jurek P, Kiefer GE, et al. Conjugation and radiolabeling of monoclonal antibodies with zirconium-89 for PET imaging using the bifunctional chelate p-isothiocyanatobenzyl-desferrioxamine. Nat Protoc 2010;5:739–43.
28. Milowsky MI, Nanus DM, Kostakoglu L, Sheehan CE, Vallabhajosula S, Goldsmith SJ, et al. Vascular targeted therapy with anti-prostate-specific membrane antigen monoclonal antibody J591 in advanced solid tumors. J Clin Oncol 2007;25:540–7.
29. Milowsky MI, Nanus DM, Kostakoglu L, Vallabhajosula S, Goldsmith SJ, Bander NH. Phase I trial of yttrium-90-labeled anti-prostate-specific membrane antigen monoclonal antibody J591 for androgen-independent prostate cancer. J Clin Oncol 2004;22:2522–31.
30. Erdi YE. Limits of tumor detectability in nuclear medicine and PET. Mol Imaging Radionucl Ther 2012;21:23–8.
31. Viola-Villegas NT, Sevak KK, Carlin SD, Doran MG, Evans HW, Bartlett DW, et al. Noninvasive imaging of PSMA in prostate tumors with (89)Zr-labeled huJ591 engineered antibody fragments: the faster alternatives. Mol Pharmaceutics 2014;11:3965–73.